第 36 卷第 3 期
2020 年 3 月

无 机 化 学 学 报
CHINESE JOURNAL OF INORGANIC CHEMISTRY

Vol.36 No.3
575-583

V_2O_5 空心球作为高效硫载体用于锂硫电池

潘沛锋 陈 平 方亚男 单 淇 陈宁娜 冯晓苗* 刘瑞卿 李 盼 马延文*
(南京邮电大学,有机电子与信息显示国家重点实验室培育基地,
先进材料研究院(IAM),有机电子与信息显示协同创新中心,南京 210023)

摘要: 以 V_2O_5 空心球作为锂硫电池的正极材料, 将其用于存储硫和限制多硫化物的穿梭效应。V_2O_5 空心球的平均直径约为 500 nm,为存储硫提供了更多空间并适应硫电极的体积变化。同时,V_2O_5 对多硫化物具有很强的化学吸附性,可以有效地限制多硫化物的穿梭效应。由于中空结构增加了硫的存储,并通过化学键牢固地吸附多硫化物,使该锂硫电池同时具有高容量和良好的稳定性。V_2O_5/S 作为正极的锂硫电池在 0.1C 倍率时显示出 1 439 mAh·g^{-1} 的高可逆容量,并在 1C 的倍率下循环 300 次后的容量约为 600 mAh·g^{-1}。

关键词: 锂硫电池; V_2O_5 空心球; 正极; 穿梭效应; 化学吸附
中图分类号: TB34 **文献标识码**: A **文章编号**: 1001-4861(2020)03-0575-09
DOI:10.11862/CJIC.2020.051

V_2O_5 Hollow Spheres as High Efficient Sulfur Host for Li-S Batteries

PAN Pei-Feng CHEN Ping FANG Ya-Nan SHAN Qi CHEN Ning-Na
FENG Xiao-Miao* LIU Rui-Qing LI Pan MA Yan-Wen*
(*Key Laboratory for Organic Electronics and Information Displays & Institute of Advanced Materials (IAM), Synergistic Innovation Center forOrganic Electronics and Information Displays, Nanjing University of Posts & Telecommunications, Nanjing* 210023, *China*)

Abstract: The V_2O_5 hollow spheres were used as a high efficient sulfur host for Li-S batteries, which was used for the storage of sulfur and restricting the shuttle effect of polysulfides. The hollow spheres had an average diameter around 500 nm, providing more space for storing sulfur, accommodating volumetric change of sulfur electrode. At the same time, V_2O_5 has a strong chemical adsorption of polysulfides, which can effectively limit the shuttle effect of polysulfides. The high capacity and excellent stability of Li-S batteries have been realized simultaneously due to the increasing of the storage of sulfur by the hollow structure and strong chemical adsorption for polysulfides by chemical bonding. The Li-S batteries with as-prepared V_2O_5/S cathode showed a high reversible capacity of 1 439 mAh·g^{-1} at 0.1C and stable cycling performance with a capacity of ~600 mAh·g^{-1} after 300 cycles at 1C.

Keywords: lithium-sulfur batteries; V_2O_5 hollow spheres; cathode; shuttle effect; chemical adsorption

In the past few decades, many significant advances have been made in the study of energy storage devices[1]. In particular, rechargeable lithium-ion batteries have a dominant position in the power market of modern electronics due to their high energy density, long cycle life, and high charge and discharge

收稿日期:2019-11-12。收修改稿日期:2019-12-25。
国家自然科学基金(No.51772157,21805140,61504062)、江苏省省自然科学基金(No.BK20150863,BK20160890)和江苏省六大人才高峰(No.2015-JY-015)资助项目。
*通信联系人。E-mail:iamxmfeng@njupt.edu.cn; iamywma@njupt.edu.cn

efficiency. However, the performance of current lithium batteries cannot meet the power supply requirements under the rapid advancement of technology. The emergence of lithium-sulfur batteries solved this problem due to its high theoretical capacity (1 675 $mAh \cdot g^{-1}$) and an energy density (2 600 $Wh \cdot kg^{-1}$)[2-4]. And the sulfur has advantages of natural richness, low cost, and non-toxicity[5]. It is possible to replace the lithium-ion batteries as the next generation battery. Despite the huge potential, lithium-sulfur batteries also have many shortcomings, such as poor conductivity of sulfur and solid polysufides produced by the reaction, that limit the utilization of sulfur during battery reactions. The polysulfides dissolved in the electrolyte will pass through the separator to the anode to affect the cycle performance of the batteries. And volume change occurs during charge and discharge process resulting in the unstable structure of sulfur cathode[6]. These disadvantages result in poor cycling performance, which prevents the commercial application of lithium-sulfur batteries.

In order to solve the above issues, many efforts have been made to explore novel structures and materials as the cathode, interlayer, electrolyte, or separator for lithium-sulfur batteries[7]. Sulfur was combined with different kinds of host materials[8], including carbon based materials, transition metal oxides, and transition metal sulfides, and so on. The carbon-based material mainly acts as a host and the baffle limit the sulfur by physical confinement [9]. Transition metal oxides have drawn extensive attention recently in view of their strong polar-polar chemical interaction with polysulfides[10]. This polar-polar chemical interaction has a great effect on suppressing the "shuttle effect" of lithium-sulfur batteries[11]. At the same time, the anchoring ability of the sulfur host material for polysulfides is also the main research direction. Therefore, designing a sulfur host material for physical and chemical adsorption for polysulfides is still a significant challenge.

Metal oxides, such as TiO_2, Ti_4O_7, and indium tin oxide can adsorb polysulfides on their inherently hydrophilic surfaces[12]. Vanadium pentoxides (V_2O_5) is a promising candidate for sulfur host materials due to its unique layered structure, excellent chemical and physical properties, wide electrochemical window, high energy efficiency, and many oxidation states[13]. Various nanostructured V_2O_5 have been used in the field of electrochemistry, such as nanowires[14], multi-shelled nanospheres[15], V_2O_5/graphene foam composite[16], nanofibers[17], surface-uneven V_2O_5 nanoparticles[18], nanosheets constructing 3D architectures[19], and so on. Among them, 3D nanostructures with hollow interiors can buffer the volume expansion leading to an enhanced cycling stability[20].

In this work, the V_2O_5 hollow spheres were synthesized by hydrothermal synthesis and annealing. V_2O_5 has a relatively large specific surface area of 26 $m^2 \cdot g^{-1}$. The hollow structure provides more space for storing sulfur, while V_2O_5 has a strong chemical adsorption of polysulfides, which can limit the shuttle effect of polysulfides. The hollow structure can also accommodate volumetric change of sulfur electrode. The prepared V_2O_5 electrode exhibited a good reversible capacity close to 600 $mAh \cdot g^{-1}$ after 300 cycles at 1C, good rate capability, and stable cycling stability.

1 Experimental

1.1 Synthesis of V_2O_5 hollow sphere

All reagents and solvents were of analytical grade and used as received without further treatment. In a typical process, 0.117 g NH_4VO_3 was added into 25 mL deionized water water with stirring. Then, 0.5 mL of 1 $mol \cdot L^{-1}$ HCl was added drop by drop, until the solution color turned orange. After that, 1.5 mL $N_2H_2 \cdot H_2O$ was added into the solution, and it was stirred for 15 min at room temperature. Then, the mixture was transferred into a teflon lined stainless steel autoclave, sealed and maintained at 120 ℃ for 4 h. After the reaction, the product was washed several times using ethanol and water, and then dried at 80 ℃ for 8 h. Last, the above product was heated in a muffle furnace with heating rate of 5 $℃ \cdot min^{-1}$ under air atmosphere at 400 ℃ for 2 h, and then cooled to room temperature naturally.

1.2 Synthesis of V_2O_5/S composites

The mixtures of the prepared V_2O_5 hollow spheres and sulfur were sealed and heated at 155 ℃ for 12 h. Then, the mixtures were heated to 250 ℃ under argon flow for 30 min in tube furnace to eliminate the sulfur on the outside surface of the V_2O_5 hollow spheres. The resulting V_2O_5/S composites with the sulfur content of 70% (*w*/*w*) were obtained, according to thermogravimetric analysis (TGA).

1.3 Characterization

XRD measurements were carried out on a Philip XRD X′PERT PRO X-ray diffractometer using Cu *Kα* radiation (λ=0.154 18 nm). The working current was 40 mA and working voltage was 40 kV with 2θ range of 15° ~70° . The structure and morphology were characterized by SEM (Hitachi S-4800, 10 kV) and TEM (Hitachi 7700, 100 kV). High-resolution TEM (HRTEM) images were recorded on FEI Talos F200X field-emission transmission electron microscope operated at 200 kV. UV-Vis adsorption spectra were recorded on a PerkinElmer UV-Vis spectrometer Lambda 650S. The valence states of elements were analyzed by X-ray photoelectron spectroscopy (PHI 5000 VersaProbe). Thermogravimetric analysis (TGA) was used to determine the sulfur content of the materials on a TGA instrument (NETZSCH STA-449 C) employing a heating rate of 10 ℃·min^{-1} from room temperature to 700 ℃ under a nitrogen flow.

CR2032-type coin cells were assembled in a glovebox filled with argon. The working electrodes were prepared by mixing 80% (*w*/*w*) active materials, 10% (*w*/*w*) acetylene black and 10% (*w*/*w*) polyvinylidene fluoride (PVDF) binder in N-methyl pyrrolidinone (NMP). The slurries were homogeneously coated onto aluminum foil current collectors. The electrodes were dried at 60 ℃ for 12 h under vacuum. Subsequently, the electrodes were cut into disks with a diameter of 13 mm. A piece of lithium foil was used for the combined counter and reference electrodes. 1.0 mol·L^{-1} lithium bis(trifluoromethanesulfonyl)imide (LiTFSI) in 1,3-dioxolane and 1,2-dimethoxyethane (volume ratio, 1∶1) with 1% (*w*/*w*) $LiNO_3$ as an additive was used as the electrolyte. The $LiNO_3$ was added to help passivate the surface of the lithium anode and reduce the "shuttle effect". Celgard 2400 was used as a separator film. The cycle performances, rate capability and galvanostatic charge/discharge tests were carried out on LAND CT2001A in a potential range of 1.5~2.8 V (vs Li/Li$^+$). The specific capacity was calculated based on the weight of sulfur. Cyclic voltammetry (CV) (scan rate: 0.2 mV·s^{-1}, cut-off voltage: 1.5 ~2.8 V) and electrochemical impedance spectra (frequency range from 100 kHz to 0.01 Hz) were measured with an electrochemical workstation VMP3.

2 Results and discussion

The precursor of V_2O_5 was fabricated using one-step hydrothermal method. The obtained precursor was heated under air atmosphere. The final porous V_2O_5 spheres could be formed after annealing. Scanning electron microscopy (SEM) images (Fig.1 (a,b)) show that the shape of precursor was uniform spheres with the average diameter around 500 nm. The spherical structure can be well maintained after annealing, as shown in Fig.1(d,e). It can be seen from the TEM images of the precursor and the obtained V_2O_5 exhibited a hollow structure with the spherical shell thickness was about ~80 nm. Compared with the precursor, the surface of the V_2O_5 hollow spheres became smooth. Fig.1(g~j) show the energy dispersive X-ray spectroscopy (EDS) elemental mappings which demonstrated the homogeneous distribution of V and O as well as sulfur inside the V_2O_5 nanospheres.

The XRD patterns of precursor and V_2O_5 are shown in Fig.2a. From the XRD pattern of precursor, it can be seen that there were no obvious diffraction peaks due to its very low crystallinity. Line b in Fig. 2a is the XRD pattern of V_2O_5 hollow spheres. All of the main diffraction peaks can be indexed and assigned to the orthogonal V_2O_5 phase (PDF No.41-1426)[21]. Raman spectrum displays the characteristic peaks of V_2O_5, as shown in Fig.2b. These vibration modes could be described to the characteristic of orthorhombic V_2O_5[22-23]. The low frequency modes at 105, 141, and 195 cm^{-1} can be attributed to external modes corresponding to the displacements of [VO_5]

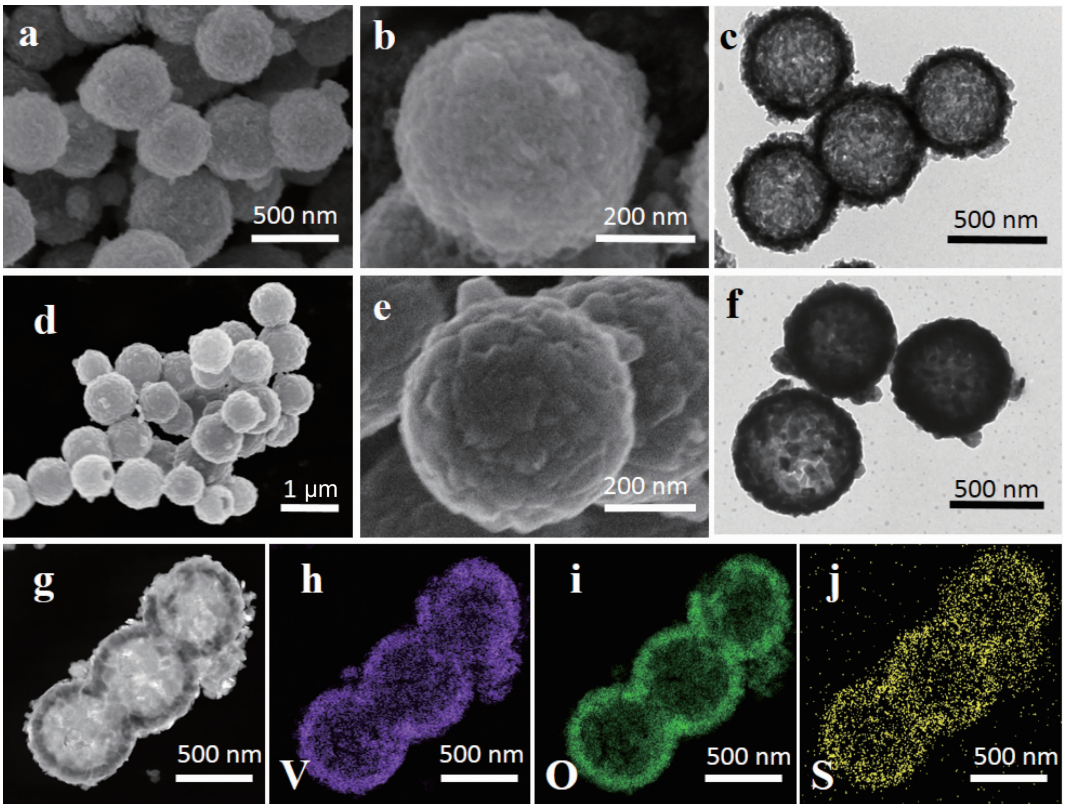

Fig.1 SEM (a, b, d, e) and TEM (c, f) images of precursor (a, b, c) and V_2O_5 (d, e, f); (g~j) Scanning transmission electron microscopy image and corresponding EDS elemental mapping images of V_2O_5/S composites

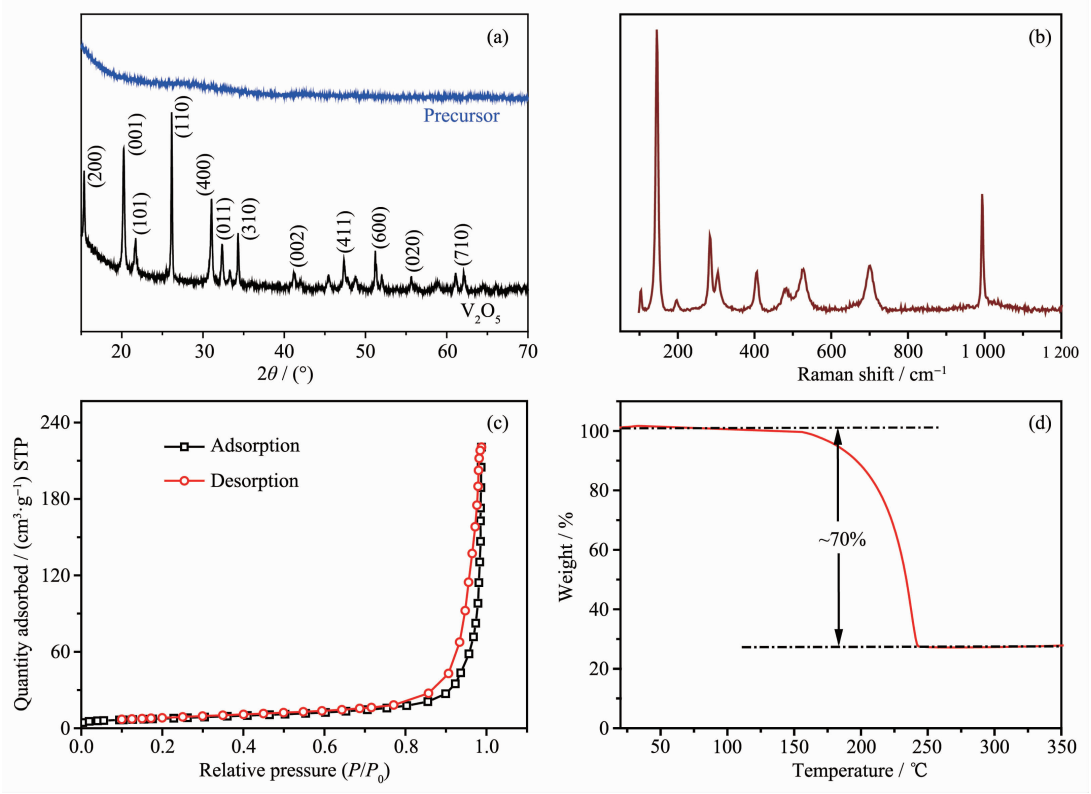

Fig.2 (a) XRD patterns of precursor and V_2O_5; (b) and (c) Raman spectrum and N_2 adsorption-desorption isotherms of V_2O_5, respcetively; (d) TGA curve of V_2O_5/S composites

units with respect to each other[24]. A sharp Raman band appeared at 995 cm^{-1} was assigned to the vanadyl stretch (V-O_1) within the VO_5 square pyramids[25]. The mode at 698 cm^{-1} was ascribed to an anti-phase stretching vibration of the V-O_2 bond. Another mode at 524 cm^{-1} was due to the stretching of inter-chain V-O_2 bonds. Two other modes at 403 and 294 cm^{-1} can be assigned to bond rocking oscillations involving the apical oxygen (O_1) atoms[26].

The specific surface area and pore volume of the V_2O_5 hollow spheres can be known by the N_2 adsorption-desorption isotherm. Fig.2c showed a sharp capillary condensation step at high relative pressure which belonged to type Ⅳ isotherm, characteristic of the presence of mesoporous material according to IUPAC classification. Brunauer-Emmett-Teller (BET) specific surface area of the as-obtained V_2O_5 hollow spheres is 26 $m^2 \cdot g^{-1}$, and the most probable distribution pore size of V_2O_5 was around 30 nm. TGA (Fig.2d) shows the sulfur content in V_2O_5/S. The TGA curve showed a weight loss between 150 and 300 ℃, which was due to the evaporation of elemental sulfur in V_2O_5/S composite materials. The mass fraction of sulfur content in the composite was about 70%(*w*/*w*).

To verify the physical trapping and strong chemical anchoring of V_2O_5 for polysulfides, an ex situ experiment of the absorption of Li_2S_6 by V_2O_5 was carried out. The orange polysulfides solution turned to colorless after adding V_2O_5 (inset in Fig.3a). As shown in Fig.3a, the peak at 300~350 nm was contributed to S_6^{2-}. It became weak after adding V_2O_5, demonstrating a good adsorption of V_2O_5 for polysulfides. In order to prove the interaction of polysulfides with V_2O_5, the chemical states of V_2O_5 and V_2O_5/Li_2S_6 were investigated by XPS, as shown in Fig.3(b~f). In Fig. 3b, the V2*p* spectrum showed two deconvoluted peaks near 524 and 517 eV, corresponding to V^{4+} and V^{5+} of the original V_2O_5, respectively[27-28]. It can be seen from Fig.3e that the two peaks of V2*p* were displaced after combining with Li_2S_6, indicating an increase in electron density at the metal element and formation of chemical bond between V_2O_5 and Li_2S_6[29]. On the one hand, the peaks of 524.4 and 516.9 eV exhibited a 0.3 and 0.7 eV shift compared to that of V_2O_5, respectively. On the other hand, the formation of the S-V bond[30] can be clearly recognized by the strong broad peaks in the range of 516~518 and 523~525 eV. Fig.3d shows the S2*p* spectrum of the V_2O_5/Li_2S_6. The peak located at 162 and 163.1 eV can be attributed to terminal (S_T^{-1}) and bridging sulfur (S_B^0), respectively[31]. In addition, a new characteristic peak at 162.5 eV emerge in S2*p* spectrum, corresponding to V-S bonds. The peak at 168.4 eV revealed V-O interaction in the V_2O_5/Li_2S_6, and the peak around 164 eV can be attributed to the S-S bond of Li_2S_6 species[32]. Two characteristic peaks of O1*s* can be observed in Fig.3c, the peak at 529.7 eV was attributed to V-O corresponding to oxidation of V based material. Besides, the peak at 531 eV corresponded to absorption of H_2O[33]. After adsorption of Li_2S_6, the total peak of O1*s* in V_2O_5/Li_2S_6 showed a large shift of about 0.4 eV to higher energy in Fig.3f, the formation of S-O bond can be clearly identified by the strong wide peak in the range of 528.5~530 eV[34]. Such results reveal a strong interaction between polysulfides species and V_2O_5[35].

The electrochemical performances of the V_2O_5/S cathode were evaluated by lithium-sulfur batteries. As shown in Fig.4a, the CV profiles of V_2O_5/S electrode was performed at a scan rate of 0.1 $mV \cdot s^{-1}$ in the potential range between 1.7 and 2.8 V vs Li^+/Li. The two prominent reduction peaks located at 2.27 and 2.03 V corresponded to the formation of soluble lithium polysulfides (Li_2S_n, $4 \leqslant n \leqslant 8$) and further reducing to short-chain insoluble lithium sulfides (Li_2S_2/Li_2S). The oxidation peak around 2.39 V can be ascribed to the conversion from Li_2S/Li_2S_2 to Li_2S_n and eventually S_8. The electrochemical impedance spectroscopy (EIS) curves of V_2O_5/S before and after CV were shown in Fig.4b. The charge-transfer resistance (R_{ct}) and the adsorption impedance (W_s) of V_2O_5/S electrode decreased sharply at 24 Ω after CV, confirming the outstanding electrocatalytic activity and the strong adsorption to the intermediate polysulfides. Importantly, the small value and stable variation of the Warburg impedance (Z_W) indicated the good

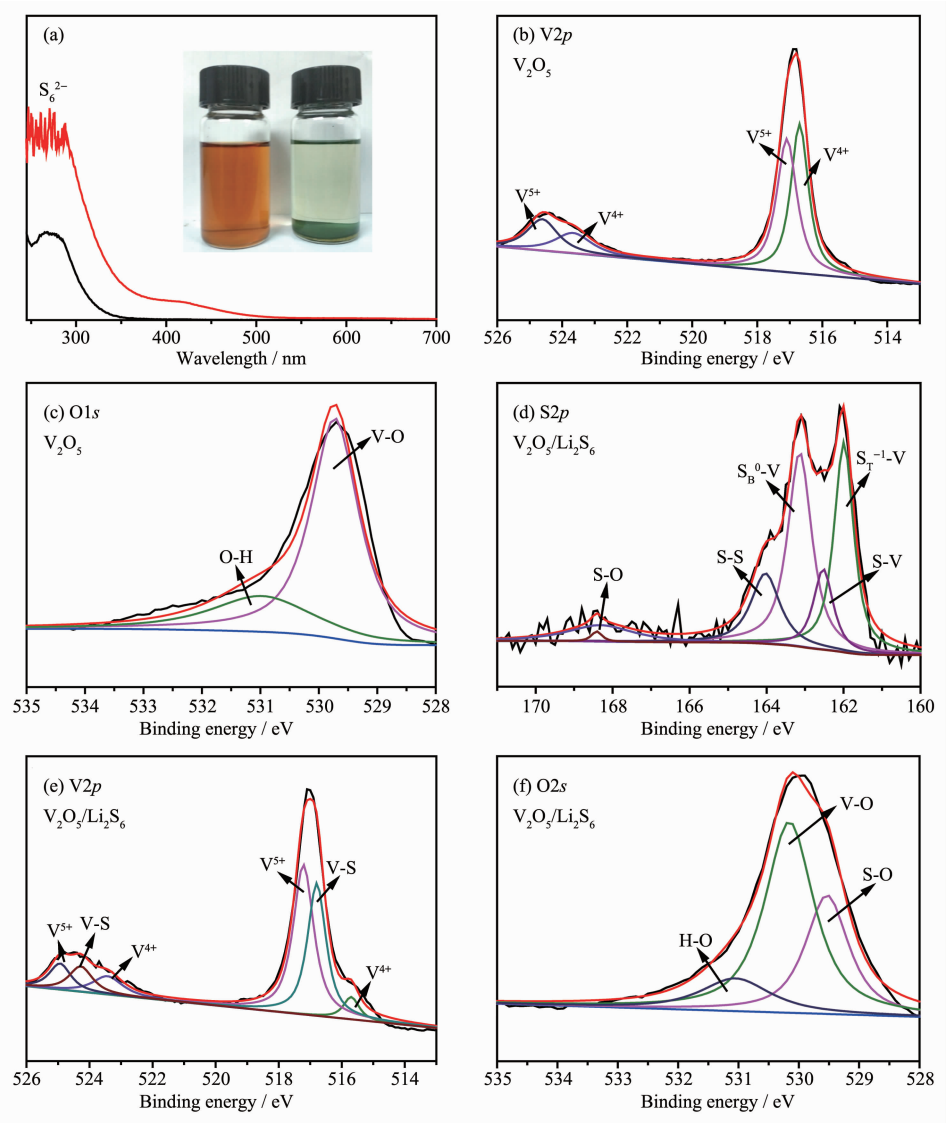

Inset in a: Digital images of Li_2S_6 and V_2O_5/Li_2S_6

Fig.3 (a) UV-Vis spectra of Li_2S_6 and V_2O_5/Li_2S_6; High-resolution XPS spectra for (b) V2*p* and (c) O1*s* of V_2O_5; High-resolution XPS spectra for (d) S2*p*, (e) V2*p* and (f) O1*s* of V_2O_5/Li_2S_6

diffusion of soluble species in the 3D framework of V_2O_5 hollow spheres in the V_2O_5/S electrode, which is indispensable and essential for the subsequent adsorption and electrocatalysis processes of soluble intermediate polysulfides[36]. As shown in Fig.4c, the reversible capacities of the V_2O_5/S electrode decreased gradually from 1 439 to 1 107, 885, 800, 654 and 507 mAh·g^{-1} with the current densities increasing from 0.1C to 3C. When the current returned back to 0.2C, the capacity can be restored to an excellent value about 950 mAh·g^{-1}, showing good stability at different current densities. As shown in Fig.4d, the well-defined charge-discharge plateaus maintained well for V_2O_5/S even at high current densities. The cathode showed a sloping charge/discharge process only when the current density reached 3C. At 0.1C, the voltage platform difference was 118 mV, that was smaller compared with other electrodes, such as reduced graphene oxide nanotubes (183 mV)[37] and Fe_2O_3 (130 mV)[38]. At 1C, the potential difference was 230 mV which was less than MnO_2 (400 mV)[39], suggesting that the electrochemical reaction reversibility of the V_2O_5/S was high. There was a relatively small polarization phenomenon of the V_2O_5/S cathode in different current densities,

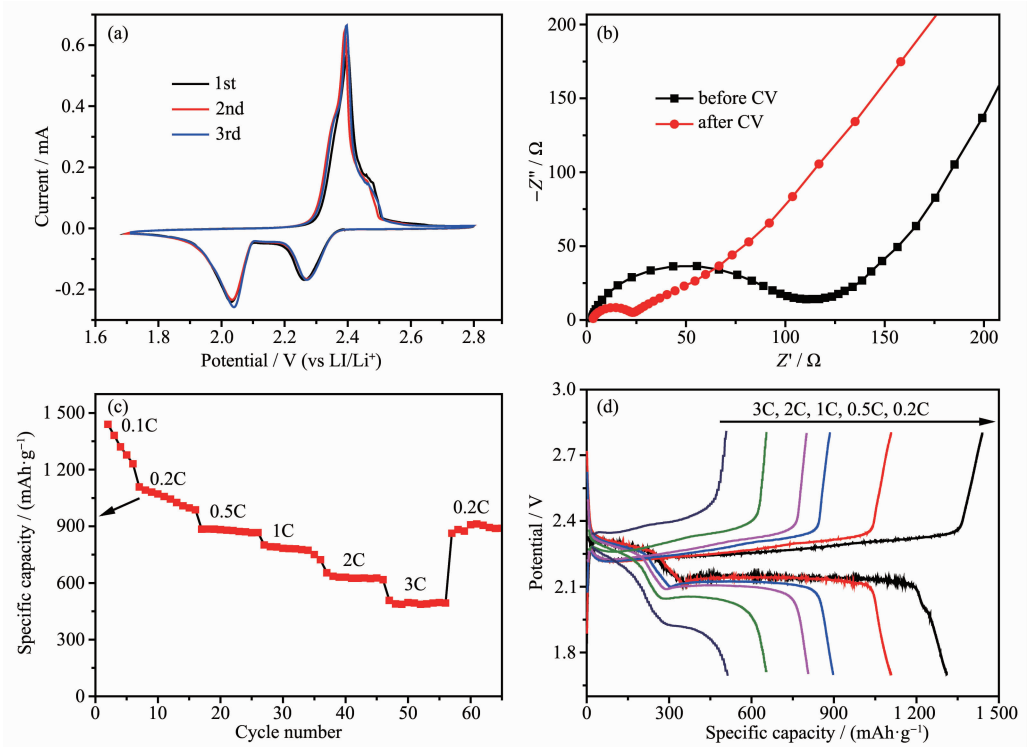

Fig.4　(a) CV curves of the first three cycles and (b) Nyquist plots of the V_2O_5/S electrode before and after CV; (c) Rate capabilities from 0.1C to 3C of V_2O_5/S electrode; (d) Discharge/charge curves during cycling at different rates

suggesting that the spherical V_2O_5 was benefit for improving the electrochemical kinetics of the sulfur cathode.

As shown in Fig.5a, CV curves at different scan rates from 0.1 to 0.4 mV·s^{-1} were further recorded to investigate the reaction kinetics and lithium diffusion properties of V_2O_5/S cathode. With the increase of the scan rate, the peak separation began to increase due to overpotential[40]. However, the peaks retained the well-defined shape even when the scan rate increased to 0.5 mV·s^{-1}. All the cathodic and anodic peak currents for the measured cathode displayed a linear relationship with the square root of scanning rates. The classical Randles-Sevcik equation can be applied to describe the Li^+ ion diffusion process: $I_p=(2.69\times105)n^{1.5}AD^{0.5}C_{Li}\nu^{0.5}$, where I_p is the peak current, n is the charge transfer number, A is the area of the active electrode, D is the lithium-ion diffusion coefficient, C_{Li} is the concentration of lithium ions in the cathode, and ν is the potential scan rate[41]. The slopes of curves in Fig.5b were positively correlated to the lithium-ion diffusion rate. Accordingly, by Randles-Sevcik equation, D of V_2O_5/S cathode for redox peak A1, C1 and C2 were calculated to be 5.42×10^{-9}, 3.37×10^{-9} and 3.29×10^{-9} cm^2·s^{-1}, respectively, implying that the presence of V_2O_5 can enhance the polysulfides redox kinetics in terms of sulfur reduction and oxidation reactions.

Fig.6a displays the cycling performance of V_2O_5/S cathode at different current densities. The beginning capacities of V_2O_5/S at 0.2C, 0.5C and 1C are 1 429, 1 014 and 805 mAh·g^{-1}. After 100 cycles, it can still remain 890, 754 and 682 mAh·g^{-1}, respectively. During cycling, the coulomb efficiencies have no obvious change, indicating that the batteries have excellent cycle performance. As shown in Fig.6c, the V_2O_5/S cathode delivered a capacity of 805 mAh·g^{-1} after activation at 0.1C for five cycles. After 300 cycles at 1C, the V_2O_5/S cathode still remains a high capacity of 584 mAh·g^{-1}, corresponding to an ultralow capacity decay of 0.24% per cycle. Due to the influence of temperature, the battery capacity

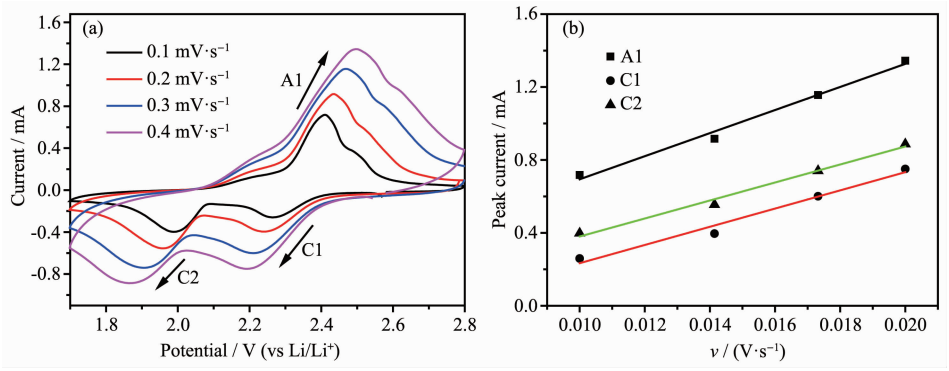

Fig.5 (a) CV curves of V_2O_5/S electrode at various scan rates and (b) the corresponding relationship between the square root of the scan rate v and peak current I_p of the V_2O_5/S electrode in a voltage range of 1.7~2.8 V vs Li^+/Li

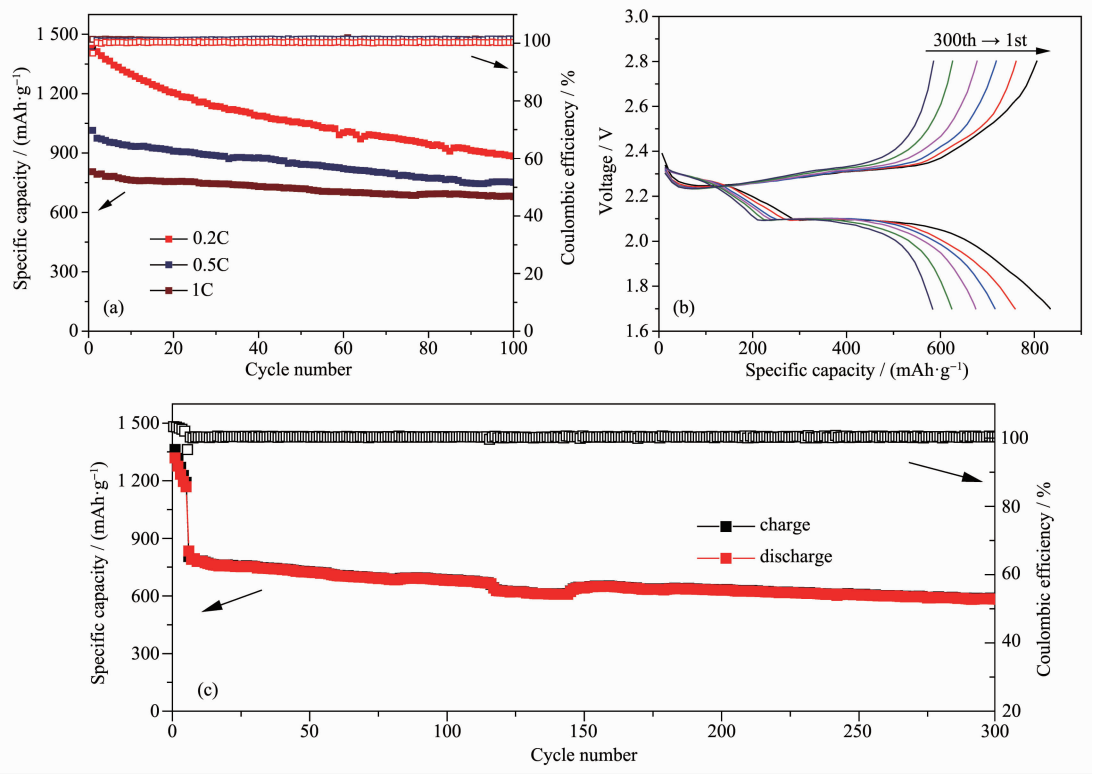

Fig.6 (a) Cycling performance of the V_2O_5/S cathode at the charge/discharge rate of 0.2C, 0.5C and 1C; (b) Galvanostatic charge-discharge voltage curves of V_2O_5/S electrode at different cycles at 1C; (c) Prolonged cycling stability of the V_2O_5/S electrode over 300 cycles at 1C

fluctuates slightly, and finally returned to the normal value, which proved that the battery has good stability. And the charge/discharge plateaus were maintained well after 300 cycles, as can be seen from Fig.6b, indicating an excellent cycling stability.

3 Conclusions

In summary, we have designed and synthesized an efficient sulfur host based on V_2O_5 hollow spheres. Due to this hollow spherical structure, this novel host not only improves the sulfur content, but also limits the expansion of the sulfur electrode. Meantime, the V_2O_5 spheres have strongly chemical adsorption for the polysulfides to improve the sulfur utilization and the cycling stability of batteries. V-S bond played critical role in effectively encapsulating of V_2O_5 on polysulfides and improve the electrochemical performances. Benefiting from the unique structure, sulfur content

was up to 70% (*w*/*w*) and remained a high capacity of 584 mAh·g^{-1} over 300 cycles at the current density of 1C.

References:

[1] Goubard-Bretesché N, Kemnitz E, Pinna N. *Mater. Chem. Front.*, **2019**,**3**:2164-2184

[2] Sun Z H, Zhang J Q, Yin L C, et al. *Nat. Comm.*, **2017**,**8**:14627-14635

[3] Zhang S T, Zheng M B, Lin Z X, et al. *J. Mater. Chem. A*, **2014**,**2**:15889-15896

[4] Ma L B, Zhang W J, Wang L, et al. *ACS Nano*, **2018**,**12**:4868-4876

[5] Manthiram A, Fu Y, Chung S H, et al. *Chem. Rev.*, **2014**, **114**:11751-11787

[6] Zhang R, Cheng X B, Zhao C Z, et al. *Adv. Mater.*, **2016**,**28**:2155-2162

[7] Xu G, Yan Q B, Kushima A, et al. *Nano Energy*, **2017**,**31**:568-574

[8] Zhang J T, Hu H, Li Z, et al. *Angew. Chem. Int. Ed.*, **2016**, **55**:3982-3986

[9] Shang C Q, Wei B B, Zhang X Z, et al. *Mater. Lett.*, **2019**, **236**:240-243

[10]Liu X, Huang J Q, Zhang Q, et al. *Adv. Mater.*, **2017**,**29**:1601759-1601784

[11]Zhang J, Yang C P, Yin Y X, et al. *Adv. Mater.*, **2016**,**28**:9539-9544

[12]Liang X, Kwok C Y, Lodi-Marzano F, et al. *Adv. Energy Mater.*, **2016**,**6**:1501636-1501645

[13]Yue Y, Liang H. *Adv. Energy Mater.*, **2017**,**7**:1602545-1602577

[14]Wang N N, Zhang Y F, Hu T, et al. *Curr. Appl. Phys.*, **2015**,**15**:493-498

[15]Wang Y P, Nie Z W, Pan A Q, et al. *J. Mater. Chem. A*, **2018**,**6**:6792-6799

[16]Ndiaye N M, Ngom B D, Sylla N F, et al. *J. Colloid Interface Sci.*, **2018**,**532**:395-406

[17]Wee G, Soh H Z, Cheah Y L, et al. *J. Mater. Chem.*, **2010**, **20**:6720-6725

[18]Zhang Y F, Zheng J Q, Wang Q S, et al. *RSC Adv.*, **2016**,**6**:93741-93752

[19]Cao A M, Hu J S, Liang H P, et al. *Angew. Chem. Int. Ed.*, **2005**,**117**:4465-4469

[20]Wang J Y, Tang H J, Zhang L J, et al. *Nat. Energy*, **2016**,**1**:1-9

[21]Enjalbert R, Galy J. *Acta Crystallogr. Sect. C*, **1986**,**42**:1467-1469

[22]Zhou B, He D Y. *J. Raman Spectrosc.*, **2008**,**39**:1475-1481

[23]Baddour-Hadjean R, Smirnov M B, Smirnov K S, et al. *Inorg. Chem.*, **2012**,**51**:3194-3201

[24]Chan C K, Peng H, Twesten R D, et al. *Nano Lett.*, **2007**,**7**:490-495

[25]Baddour-Hadjean R, Pereira-Ramos J P. *Chem. Rev.*, **2010**, **110**:1278-1319

[26]Horrocks G A, Likely M F, Velazquez J M, et al. *J. Mater. Chem. A*, **2013**,**1**:15265-15277

[27]Swiatowska-Mrowiecka J, Maurice V, Zanna S, et al. *Electrochim. Acta*, **2007**,**52**:5644-5653

[28]Benayad A, Martinez H, Gies A, et al. *J. Electron. Spectrosc.*, **2006**,**150**:1-10

[29]Rao Y, Zhang L M, Shang X, et al. *Appl. Surf. Sci.*, **2017**,**423**:1090-1096

[30]Rout C S, Kim B H, Xu X, et al. *J. Am. Chem. Soc.*, **2013**, **135**:8720-8725

[31]Wang Y K, Zhang R F, Chen J, et al. *Adv. Energy. Mater.*, **2019**,**9**:1900953-1900964

[32]Zhu L, Li C C, Ren W J, et al. *New J. Chem.*, **2018**,**42**:5109-5116

[33]Kotsis K, Staemmler V. *Phys. Chem. Chem. Phys.*, **2006**,**8**:1490-1498

[34]Xue W, Yan Q B, Xu G, et al. *Nano Energy*, **2017**,**38**:12-18

[35]Liu F, Chen Z X, Fang G Z, et al. *Nano-Micro Lett.*, **2019**, **11**:25-36

[36]Wang Z Y, Wang L, Liu S, et al. *Adv. Funct. Mater.*, **2019**, **29**:1901051-1901061

[37]Chen K, Cao J, Lu Q Q, et al. *Nano Res.*, **2017**,**11**:1345-1357

[38]Cao Z X, Jia J Y, Chen S N, et al. *ACS Appl. Mater. Interfaces*, **2019**,**11**:39772-39781

[39]Kim K, Kim P J, Youngblood J P, et al. *Chem. Sus. Chem.*, **2018**,**11**:2375-2381

[40]Tang W, Liu L L, Tian S, et al. *Electrochem. Commun.*, **2010**,**12**:1524-1526

[41]Zhou G M, Tian H Z, Jin Y, et al. *Proc. Natl. Acad. Sci. USA*, **2017**,**114**:840-845